Modeling the interinfluence of fertilizer-induced NH_3 emission, nitrogen deposition, and aerosol radiative effects using modified CESM2

Ka Ming Fung[1,a], Maria Val Martin[2], Amos P. K. Tai[1,3]

[1] Graduate Division of Earth and Atmospheric Sciences, The Chinese University of Hong Kong, Sha Tin, Hong Kong
[2] Leverhulme Centre for Climate Change Mitigation, Department of Animal & Plant Sciences, University of Sheffield, Sheffield, UK
[3] Institute of Environment, Energy and Sustainability, and State Key Laboratory of Agrobiotechnology, The Chinese University of Hong Kong, Sha Tin, Hong Kong
[a] Now at: Department of Civil and Environmental Engineering, Massachusetts Institute of Technology, Cambridge, MA, USA

Correspondence to: Ka Ming Fung (kamingfung@link.cuhk.edu.hk) & Amos P. K. Tai (amostai@cuhk.edu.hk)

Supplementary Information

1. Soil structure

Table S1. Soil layer structure.

Layer#	Layer Node Depth l (m)	Layer Thickness Δl (m)	Weighting Factor $e^{(-10l)/\Delta l}$	Nitrogen Distribution Fraction
1	0.01	0.02	45.2	62.8%
2	0.04	0.04	16.8	23.3%
3	0.09	0.06	6.8	9.4%
4	0.16	0.08	2.5	3.5%
5	0.26	0.12	0.6	0.9%
6	0.40	0.16	0.1	0.2%
7	0.58	0.20	0.0	-
8	0.80	0.24	0.0	-
9	1.06	0.28	0.0	-
10	1.36	0.32	0.0	-
11	1.70	0.36	0.0	-
12	2.08	0.40	0.0	-
13	2.50	0.44	0.0	-
14	2.99	0.54	0.0	-
15	3.58	0.64	0.0	-
16	4.27	0.74	0.0	-

17	5.06	0.84	0.0	-
18	5.95	0.94	0.0	-
19	6.94	1.04	0.0	-
20	8.03	1.14	0.0	-
21	9.80	2.39	0.0	-
22	13.33	4.68	0.0	-
23	19.48	7.64	0.0	-
24	28.87	11.14	0.0	-
25	42.00	15.12	0.0	-

Reference:

- Section 2.2.2 in CLM5 technical notes, https://escomp.github.io/ctsm-docs/versions/release-clm5.0/html/tech_note/Ecosystem/CLM50_Tech_Note_Ecosystem.html, accessed on Jul 29, 2021
- Source code of CLM5: https://github.com/ESCOMP/CTSM/blob/master/src/soilbiogeochem/SoilBiogeochemVerticalProfileMod.F90, accessed on Jul 29, 2021

2. Canopy capture

Figure S1 shows the time series of the fractional amount of NH_3 captured by above-ground crop biomass. Our scheme showed that crops do not capture as much NH_3 as natural vegetation (~60–80% as estimated in our scheme) due to their smaller canopies, except for sugarcane and temperate soybean, which can retain >30% of NH_3 emitted. CLM5 allows crops to be irrigated or rainfed. We observed a general trend that irrigated crops retain more soil NH_3 emission than rainfed ones, which can be explained by their higher in-canopy air humidity. Despite instantaneous values varying with plant growth, our calculated canopy capture fractions are close to those used in previous studies (e.g., Bouwman et al., 1997), i.e., 20% for other shrubs, grasses, and crops.

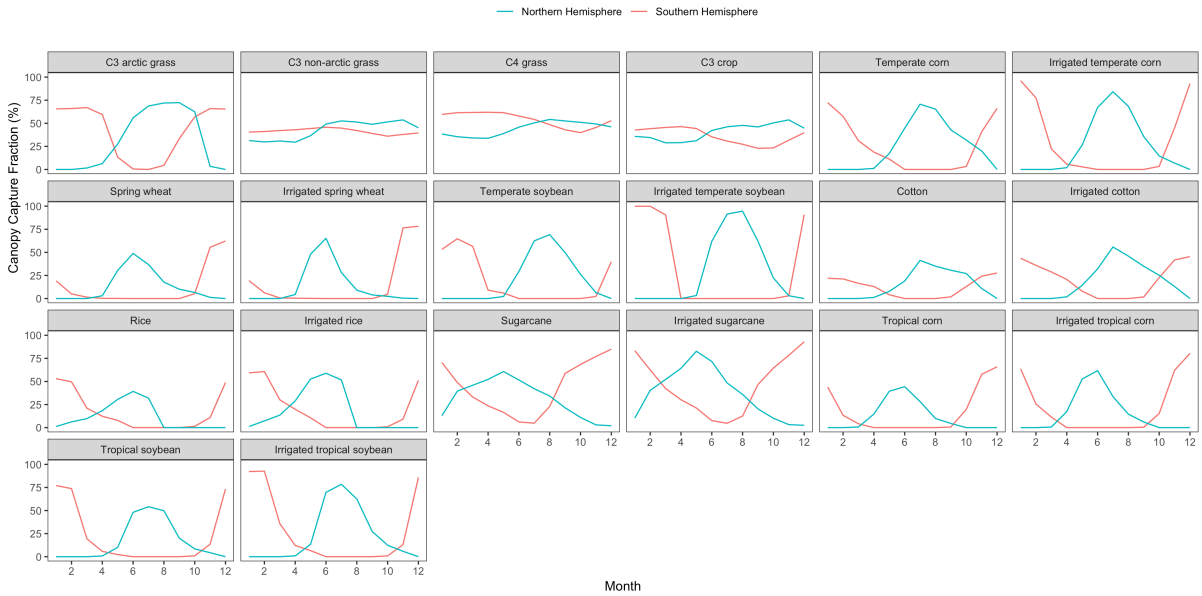

30 **Figure S1.** Monthly global-mean fractions of NH_3 captured (%) by each PFT canopy in each hemisphere.

Table S2. Annual mean fraction of NH3 captured (%) by PFTs.

Crops	**%NH_3 Captured**
Temperate corn	24.8
Irrigated temperate corn	27.1
Spring wheat	12.7
Irrigated spring wheat	14.5
Temperate soybean	19.9
Irrigated temperate soybean	30.1
Cotton	13.2
Irrigated cotton	19.7
Rice	14.3
Irrigated rice	19.0
Sugarcane	37.2
Irrigated sugarcane	41.2
Tropical corn	14.5
Irrigated tropical corn	18.6
Tropical soybean	19.3
Irrigated tropical soybean	25.4

3. Sensitivity to soil pH

CLM5 does not have a built-in method to compute soil pH implicitly. Thus, in **Results**, we used a constant global pH of 6.5, based on the implementation of the NH_3 volatilization scheme in DNDC (Li et al., 2012), to avoid the uncertain and highly spatial varying soil acidity. We tested the sensitivity of our simulated NH_3 emission by using the soil pH map from the Harmonized World Soil Database (HWSD) v1.2 (Wieder, 2014) showed in **Figure S2(c)**. This soil pH dataset shows that the middle 50% of soil has pH values ranged from 5.4–7.0. When comparing maps in **Figure S2(b)** and **(c)**, we observed that the more alkaline the soil is, the more soil emits NH_3. From our scheme (**Eq. (3)** in particular) for NH_3 volatilization, the emission rate is of the order of 10^{pH}:

$$\frac{\mathrm{d}[\mathrm{NH_{3\,(g)}}]}{\mathrm{d}t}_{\mathrm{soil}} \sim O\left(\frac{K_{\mathrm{w}}}{10^{-\mathrm{pH}}K_{\mathrm{a}}}\right) \sim O'(10^{\mathrm{pH}}) \quad \text{(S1)}$$

Figure S2(d) also illustrates and confirms this exponential relation between NH_3 emission and pH, pointing to a demand for an implicit approach for calculating prognostic soil alkalinity. Current version of CLM5 tracks only a few chemicals in soil, including NH_4^+, NO_3^-, and methane (CH_4), making the calculation of bulk soil pH difficult. Future models shall include crucial chemicals and processes, as characterized by experimental studies, that affect soil pH.

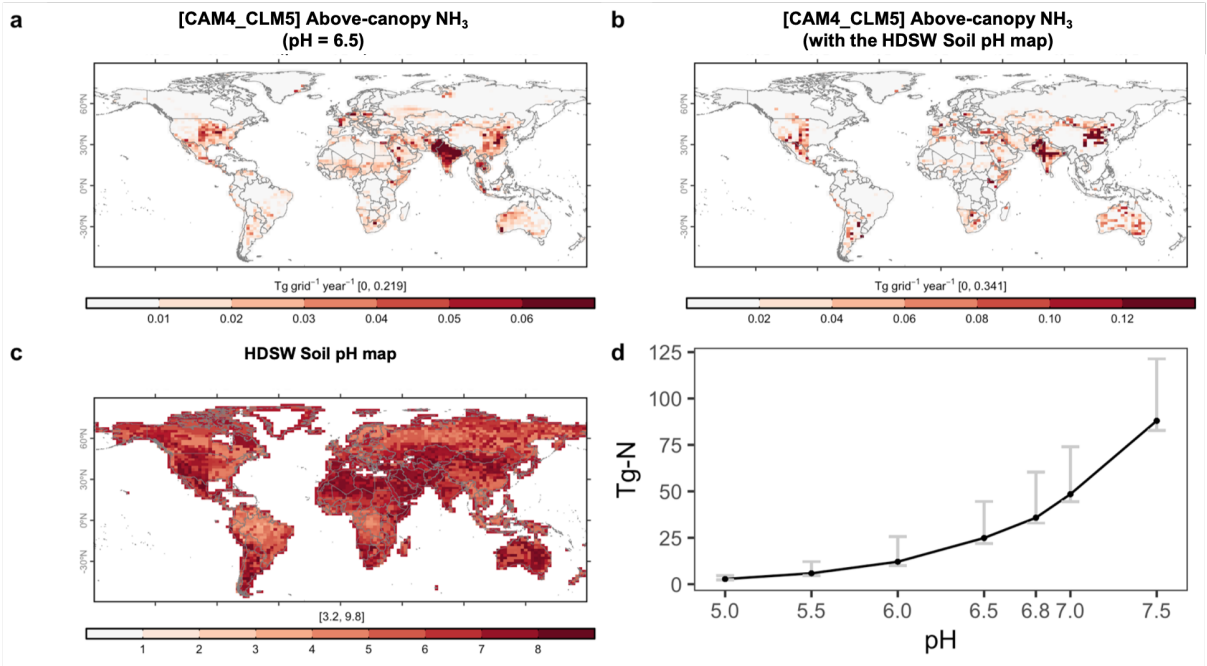

Figure S2. CLM5-simulated global soil NH_3 emission at above-canopy level with **(a)** a constant global pH of 6.5, and; **(b)** a spatially varying pH map re-gridded from the Harmonized World Soil Database v1.2 (HWSD) (Wieder, 2014), which is shown in map **(c)**. Graph **(d)** shows the total soil NH_3 emission against various global pH values from 5.0 to 7.5. Error bars indicate the maxima and minima across five of simulation.

4. Modifications to CLM5 for modeling other reactive nitrogen

In addition to the NH_3 schemes, we also incorporated new equations to calculate NO_x released as by-products of nitrification and denitrification. The original CLM5 estimates the amount of N_2O leakage during nitrification by applying a constant scaling factor to the nitrification rate (Li et al., 2000) while that from denitrification is variable and evaluated by the DayCent approach (Del Grosso et al., 2000). Building on the work of previous studies (Parton et al., 2001, 2004; Zhao et al., 2017), we computed a ratio of NO_x to N_2O to account for the leaking of the former during nitrification and denitrification using the following equations:

$$NO_x{:}\,N_2O = 15.2 + \frac{35.5\tan^{-1}[0.68\pi(10D_r - 1.86)]}{\pi} \quad \text{(S2)}$$

where D_r is the relative gas diffusivity in soil vs. in air and is calculated as a function of air-filled pore space (AFPS) of soil (Davidson and Trumbore, 1995):

$$D_r = 0.209\mathrm{AFPS}^{\frac{4}{3}} \quad \text{(S3)}$$

$$\mathrm{AFPS} = 1 - \frac{\theta_V}{\theta_{V,sat}} \quad \text{(S4)}$$

where θ_V and $\theta_{V,sat}$ are instantaneous and saturated volumetric soil water content (in $m^3\ m^{-3}$), respectively.

In addition, we added back the 20% of microbial mineralized nitrogen to the nitrification rate, which was missing in the previous versions of CLM, following the DayCent approach (Parton et al., 2001). We also applied a temperature factor to correct the overestimation of NO_x emission at high latitudes as suggested in some previous studies (Xu and Prentice, 2008; Zhao et al., 2017):

$$f_T = \min\left(1, e^{308.56\left(\frac{1}{68.02} - \frac{1}{T_{soil}+46.02}\right)}\right) \quad \text{(S5)}$$

where T_{soil} is soil temperature measured in Kelvin (K) here.

5. Supplementary figures to Section 3.2

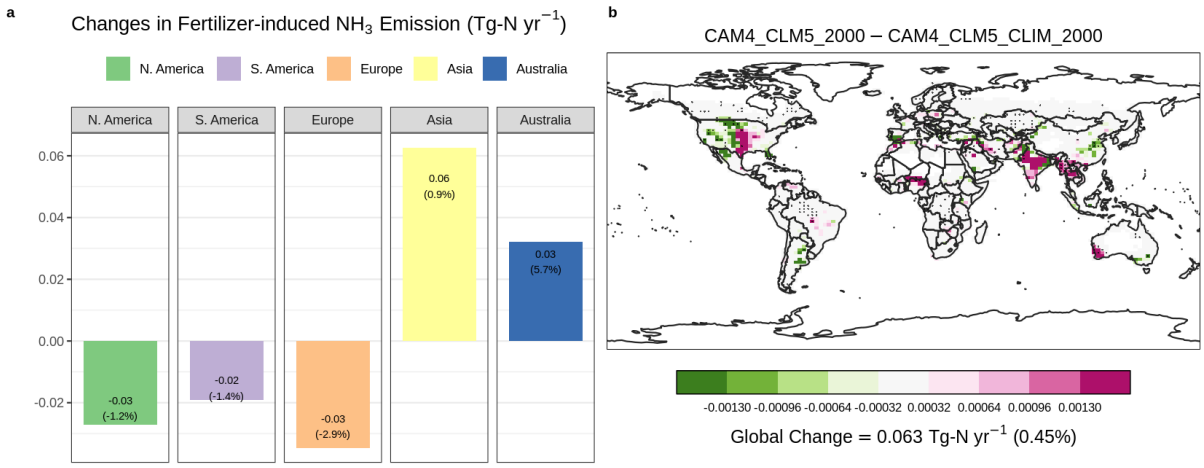

Figure S3. Contrasting annual-total fertilizer-induced NH_3 estimated by fully coupled CAM4-chem with online CLM5 NH_3 emission and NH_y deposition ([CAM4_CLM5_2000]), and CAM4-chem with online CLM5 NH_3 and prescribed NH_y deposition ([CAM4_CLM5_CLIM_2000]) at 2000-level fertilization. The prescribed NH_y map in [CAM4_CLM5_CLIM_2000] is from the monthly average of [CAM4_CLM5_2000] over 20 years. Panel **(a)** summarizes the regional differences of annual-total NH_3 emission between the two cases ([CAM4_CLM5_2000]–[CAM4_CLM5_CLIM_2000]). Panel **(b)** shows the spatial distribution of their differences.

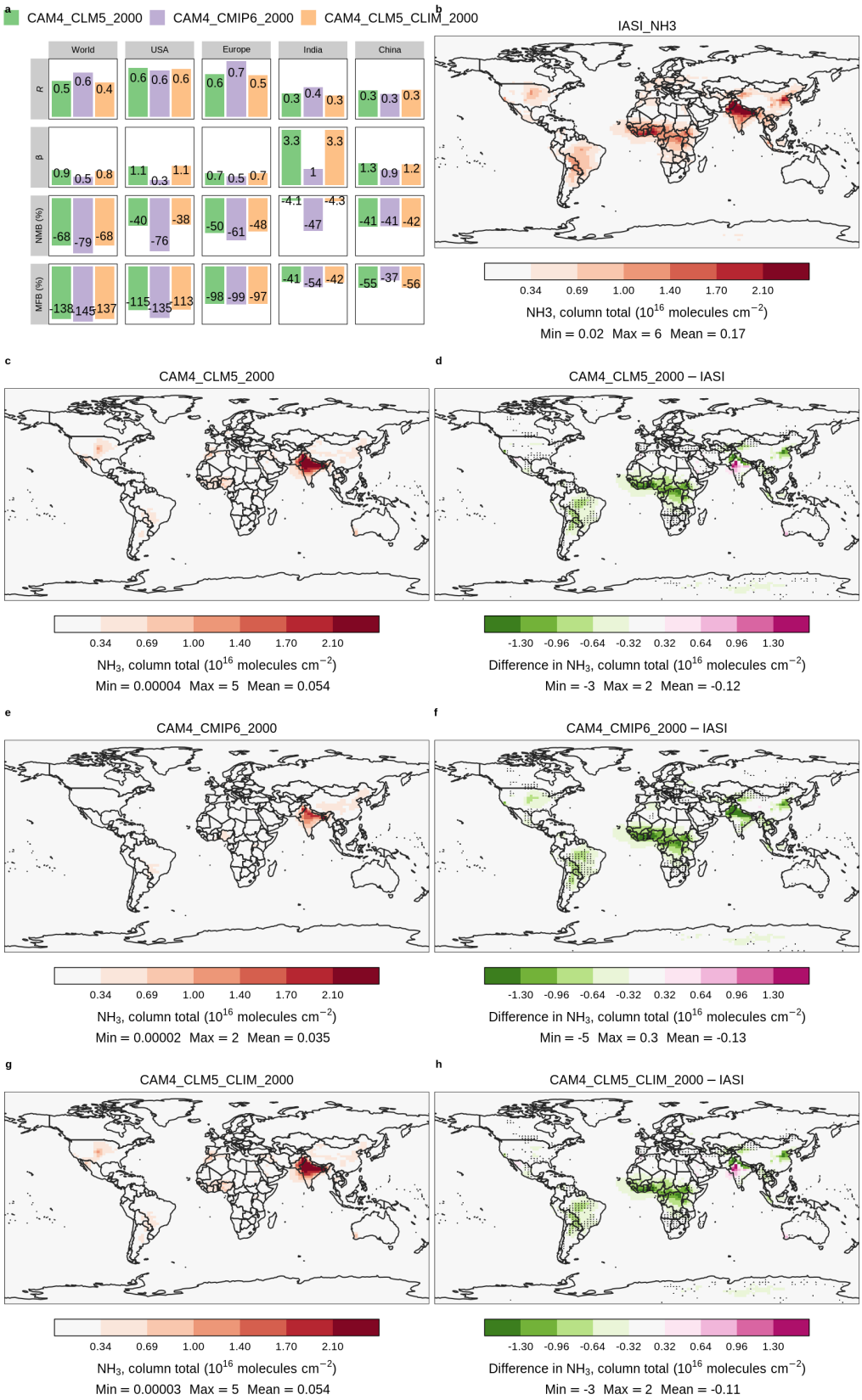

Figure S4. Annual-mean atmospheric NH_3 estimated by fully coupled CAM4-chem with online CLM5 NH_3 emission and NH_y deposition ([CAM4_CLM5_2000]), CAM4-chem with fertilizer-induced NH_3 emission from CMIP6 emission inventory and online NH_y deposition ([CAM4_CMIP6_2000]), and CAM4-chem with online

CLM5 NH_3 and prescribed NH_y deposition ([CAM4_CLM5_CLIM_2000]) at 2000-level fertilization. The prescribed NH_y map in [CAM4_CLM5_CLIM_2000] is from the monthly average of [CAM4_CLM5_2000] over 5 years. Panel **(a)** summarizes correlation analysis between the three cases and the IASI satellite retrievals. Panels **(b)**, **(c)**, **(e)**, and **(g)** show the column NH_3 concentration of IASI and the three simulation cases correspondingly. Panels **(d)**, **(f)** and **(h)** show concentration differences between each case and the IASI observations. Overlaying black dots indicate grid-cells with a statistically significant difference under two-sample t-tests (i.e., p <0.05) between corresponding simulations. Color scales are saturated at respective values, and ranges of values are shown in the legend titles.

6. Supplementary figures and table to Section 3.3

Table S3. Summary of N fluxes in the simulations averaged over 20 years.

	Fertilization (Tg-N yr^{-1})	**Plant Uptake (Tg-N yr^{-1})**	**Plant Uptake to Fertilization (%)**
CAM4_CLM5_2000	96.5	127	132
CAM4_CLM5_2050	117.0	135	115
CAM4_CLM5_CLIM_2050	117.0	133	114
CAM4_CLM5_NDEP_2050	117.0	135	115

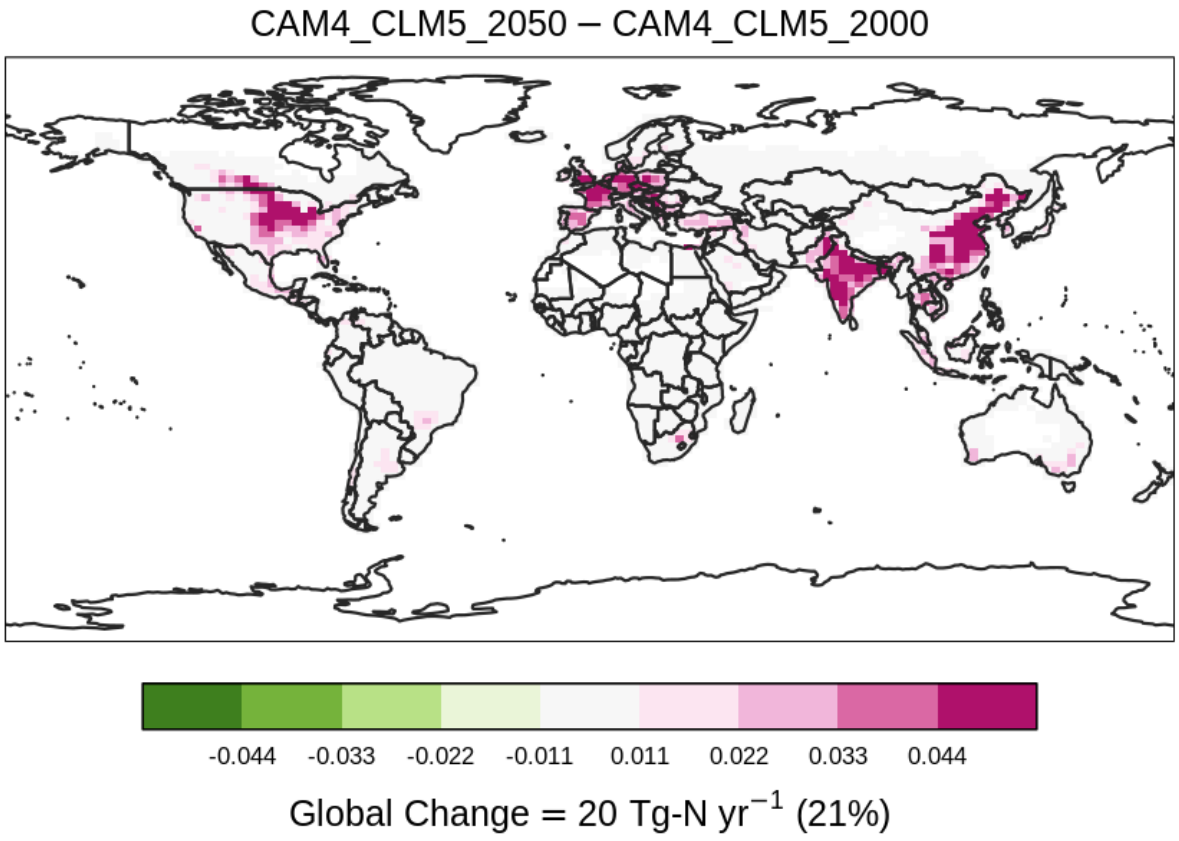

105

Figure S5. Changes in annual-total fertilizer N input to the soil (Tg-N yr^{-1}) after an 30% additional synthetic fertilizer is applied from [CAM4_CLM5_2000] to [CAM4_CLM5_2050]. Color scales are saturated at respective values.

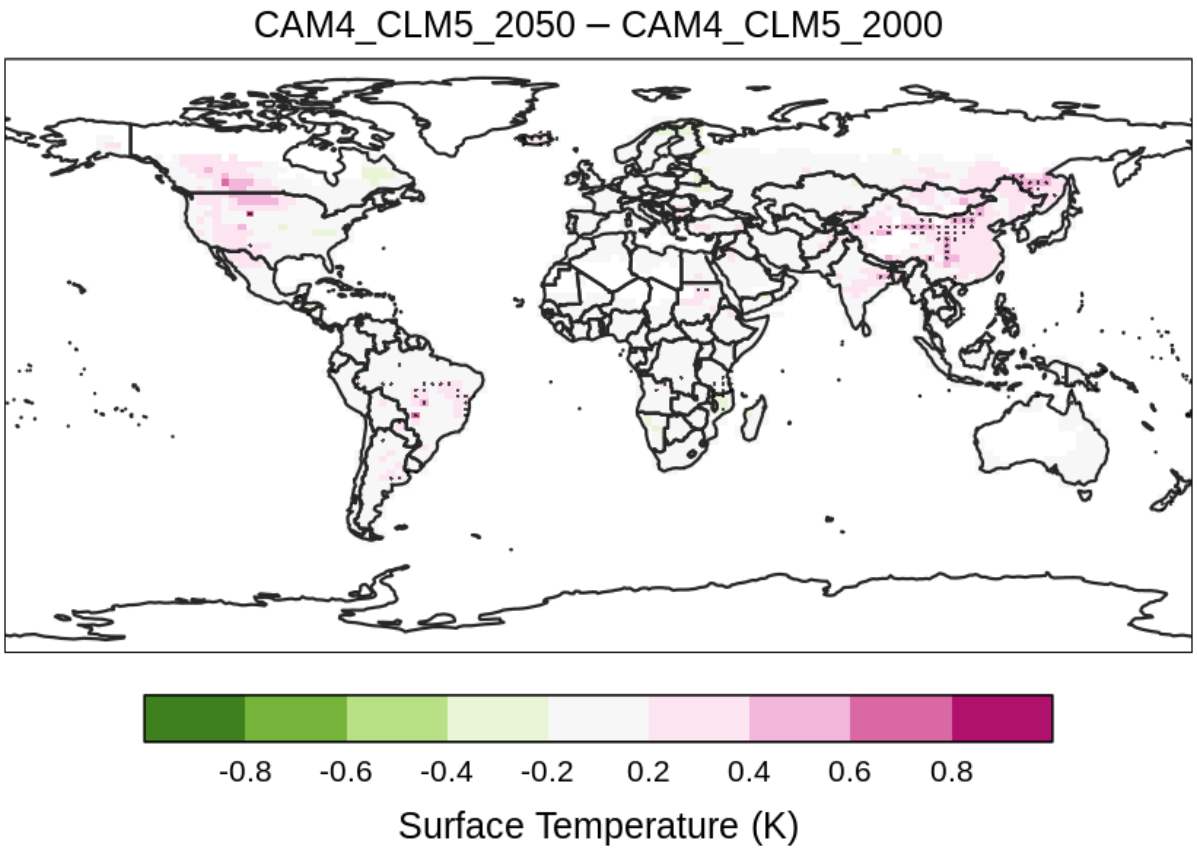

Figure S6. Contrasting the surface temperature (K). Overlaying black dots indicate grid-cells with a statistically significant difference under two-sample t-tests (i.e., p <0.05) between corresponding simulations. Only results of grid-cells with croplands are shown.

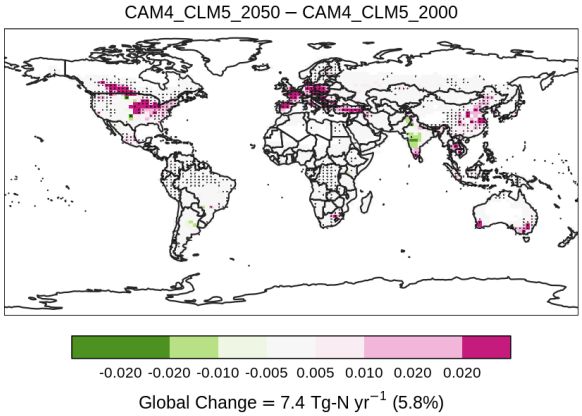

115

Figure S7. Changes in annual-total crop N uptake (Tg-N yr^{-1}) after a 30% fertilization increase from [CAM4_CLM5_2000] to [CAM4_CLM5_2050]. Overlaying black dots indicate grid-cells with a statistically significant difference under two-sample t-tests (i.e., p <0.05) between corresponding simulations. Color scales are saturated at respective values.

120

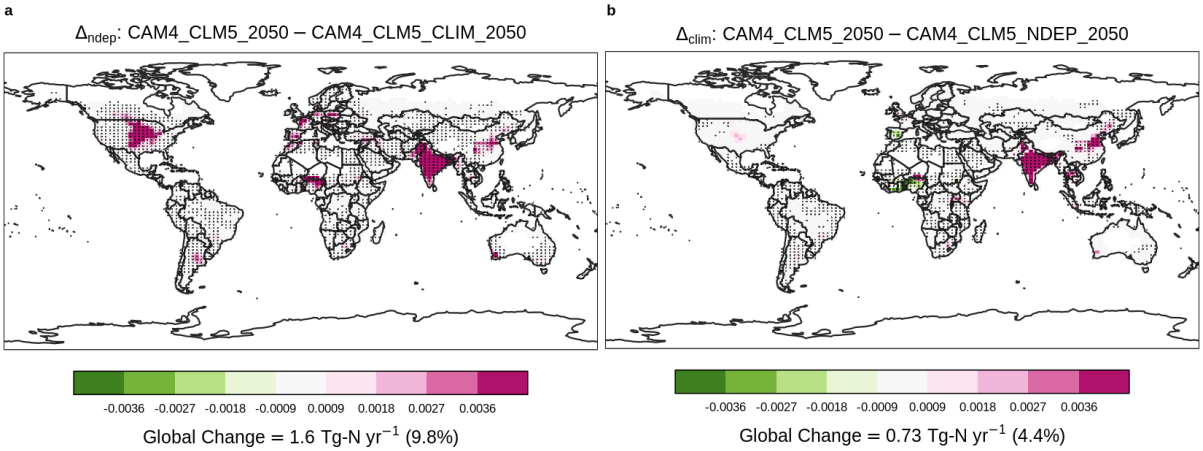

Figure S8. Contrasting the changes in nitrogen (N) deposition (Tg-N yr^{-1}). Overlaying black dots indicate grid-cells with a statistically significant difference under two-sample t-tests (i.e., p <0.05) between corresponding simulations. Only results of grid-cells with croplands are shown.

125

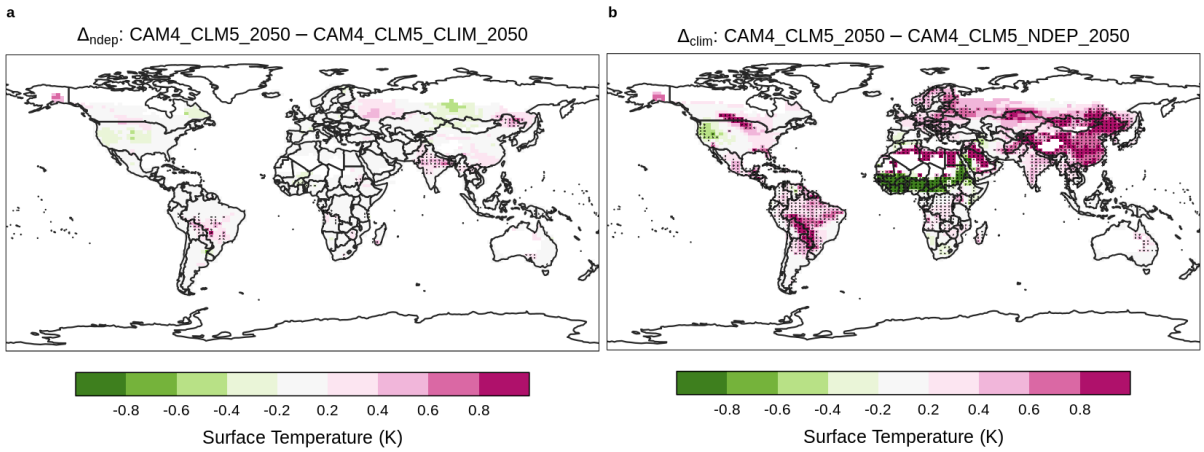

Figure S9. Contrasting the changes in annual-mean surface temperature (K). Overlaying black dots indicate grid-cells with a statistically significant difference under two-sample t-tests (i.e., p <0.05) between corresponding simulations. Only results of grid-cells with croplands are shown.

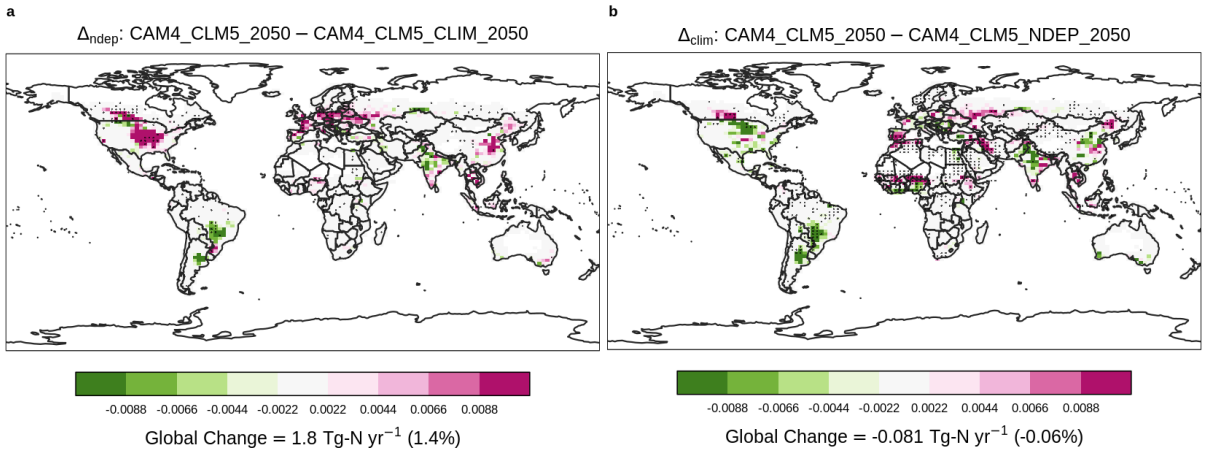

Figure S10. Contrasting the changes in plant nitrogen uptake (Tg-N yr^{-1}). Overlaying black dots indicate grid-cells with a statistically significant difference under two-sample t-tests (i.e., p <0.05) between corresponding simulations. Only results of grid-cells with croplands are shown.

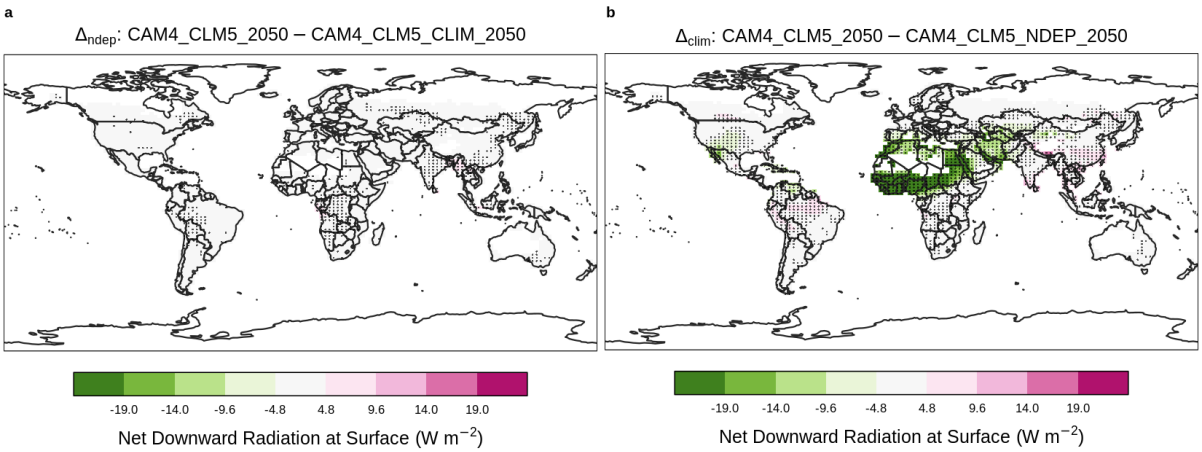

Figure S11. Contrasting the changes in annual-mean net downward radiation at surface (W m^{-2}). Overlaying black dots indicate grid-cells with a statistically significant difference under two-sample t-tests (i.e., p <0.05) between corresponding simulations. Only results of grid-cells with croplands are shown.

140

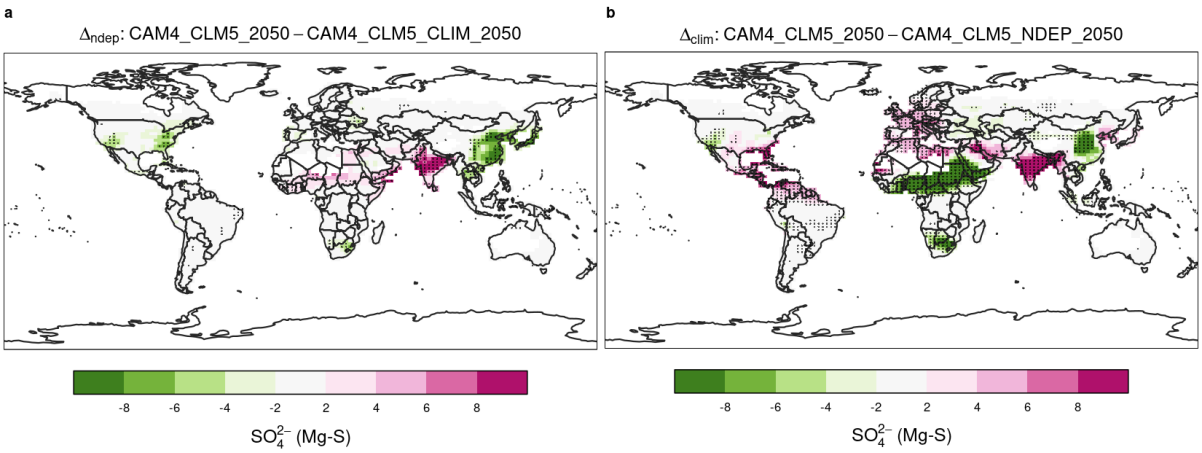

Figure S12. Contrasting the changes in annual-mean column burden of particulate sulfate. Overlaying black dots indicate grid-cells with a statistically significant difference under two-sample t-tests (i.e., p <0.05) between corresponding simulations. Only results of grid-cells with croplands are shown.

145

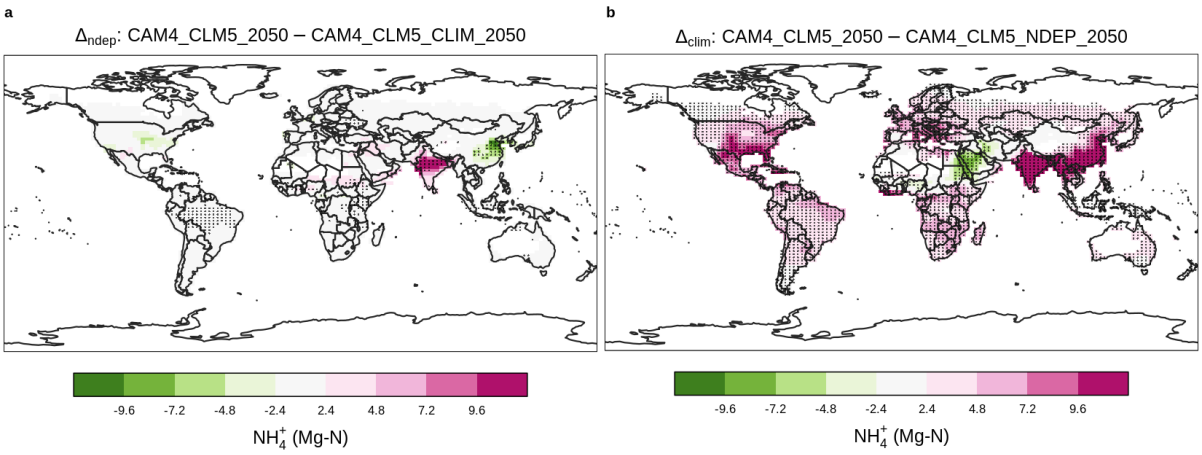

Figure S13. Contrasting the changes in annual-mean column burden of particulate NH_4^+. Overlaying black dots indicate grid-cells with a statistically significant difference under two-sample t-tests (i.e., p <0.05) between corresponding simulations. Only results of grid-cells with croplands are shown.

150

Reference

Bouwman, A. F., Lee, D. S., Asman, W. A. H., Dentener, F. J., Van Der Hoek, K. W., and Olivier, J. G. J.: A global high-resolution emission inventory for ammonia, 11, 561–587, https://doi.org/10.1029/97GB02266, 1997.

Davidson, E. A. and Trumbore, S. E.: Gas diffusivity and production of CO2 in deep soils of the eastern Amazon, 47, 550–565, https://doi.org/10.1034/j.1600-0889.47.issue5.3.x, 1995.

Del Grosso, S. J., Parton, W. J., Mosier, A. R., Ojima, D. S., Kulmala, A. E., and Phongpan, S.: General model for N2O and N2 gas emissions from soils due to dentrification, 14, 1045–1060, https://doi.org/10.1029/1999GB001225, 2000.

Li, C., Aber, J., Stange, F., Butterbach-Bahl, K., and Papen, H.: A process-oriented model of N 2 O and NO emissions from forest soils: 1. Model development, 105, 4369–4384, https://doi.org/10.1029/1999JD900949, 2000.

Li, C., Salas, W., Zhang, R., Krauter, C., Rotz, A., and Mitloehner, F.: Manure-DNDC: A biogeochemical process model for quantifying greenhouse gas and ammonia emissions from livestock manure systems, 93, 163–200, https://doi.org/10.1007/s10705-012-9507-z, 2012.

Parton, W. J., Holland, E. A., Del Grosso, S. J., Hartman, M. D., Martin, R. E., Mosier, A. R., Ojima, D. S., and Schimel, D. S.: Generalized model for NO_x and N_2O emissions from soils, 106, 17403–17419, https://doi.org/10.1029/2001JD900101, 2001.

Parton, W. J., Holland, E. A., Del Grosso, S. J., Hartman, M. D., Martin, R. E., Mosier, A. R., Ojima, D. S., and Schimel, D. S.: Generalized model for NO x and N 2 O emissions from soils , 106, 17403–17419, https://doi.org/10.1029/2001jd900101, 2004.

Wieder, W.: Regridded Harmonized World Soil Database v1.2, https://doi.org/10.3334/ornldaac/1247, 2014.

Xu, R. and Prentice, I. C.: Terrestrial nitrogen cycle simulation with a dynamic global vegetation model, 14, 1745–1764, https://doi.org/10.1111/j.1365-2486.2008.01625.x, 2008.

Zhao, Y., Zhang, L., Tai, A. P. K., Chen, Y., and Pan, Y.: Responses of surface ozone air quality to anthropogenic nitrogen deposition in the Northern Hemisphere, 17, 9781–9796, https://doi.org/10.5194/acp-17-9781-2017, 2017.